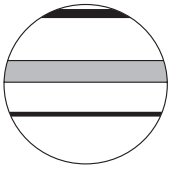

Research paper

Late-Holocene subtropical mangrove dynamics in response to climate change during the last millennium

The Holocene
1–12

DOI: 10.1177/0959683618816438
journals.sagepub.com/home/hol
SAGE

Marlon C França,[1,2,3] Luiz CR Pessenda,[2] Marcelo CL Cohen,[3] Allana Q de Azevedo,[3] Neuza A Fontes,[3] Fernando Borges Silva,[3] João CF de Melo Jr,[4] Marisa de C Piccolo,[3] José A Bendassolli[3] and Kita Macario[5]

Abstract

This work aims to study the impacts of climate change in the subtropical mangroves during the late-Holocene on a southern Brazilian coastal plain and discuss the environmental conditions to the mangrove establishment near the austral limit of South America mangroves. Samples were collected to study palynological groups, sedimentary facies, and geochemistry analyses ($\delta^{13}C$, $\delta^{15}N$, TOC, TN, C:N ratio, TS, and C:S ratio), synchronized with four radiocarbon ages. The main result of this research was the mangrove succession, divided into three palynological zones composing two facies association: (1) herbaceous tidal flat and (2) mangrove tidal flat. The first zone between at least ~1815 and ~1629 cal. yr BP was marked by the mangrove absence with marine particulate organic carbon, C_3 terrestrial plants, and macrophytes organic matter influence with $\delta^{13}C$ values between −26.7‰ and −20‰, $\delta^{15}N$ values $\bar{x} = 3.5$‰ and C:N around 21.8. The second zone between ~1629 and ~853 cal. yr BP was marked by the mangrove establishment represented only by *Laguncularia* pollen under influence of estuarine organic matter ($\delta^{13}C$ $\bar{x} = -26.5$‰; $\delta^{15}N$ $\bar{x} = 3.2$‰, and C:N around 16.4). The third zone reveals an increase of *Laguncularia* and presence of *Avicennia* pollen since ~853 cal. yr BP. Near the surface (<10 cm) occurs *Rhizophora* pollen, indicating the establishment of this genus during the past decades, under the modern environmental condition ($\delta^{13}C$ $\bar{x} = -27.02$‰; $\delta^{15}N$ $\bar{x} = 3.12$‰, and C:N around 17.42). This mangrove vertical succession may be associated with the low-temperature tolerance, where the sequence *Rhizophora, Avicennia*, and *Laguncularia* occurs from the northern to the southern limits of Santa Catarina coast, respectively, reflecting the temperature gradient. Therefore, probably, the establishment of the mangrove assemblage identified along the studied pollen profile was influenced by a temperature increase of air and water during the late-Holocene and, considering the *Rhizophora* genus, only during the past decades.

Keywords

carbon and nitrogen isotopes, palynology, sedimentary features, South America

Received 15 May 2018; revised manuscript accepted 15 October 2018

Introduction

Climate change is altering the biosphere, in marine and terrestrial environments, on large and small scales (Flantua et al., 2016; Hannah and Bird, 2018; Mayle et al., 2000). In coastal areas, sea-level rise, rising air temperatures, and changing rainfall regimes elicit short- and long-term changes in vegetation by altering physical conditions that affect the survival, distribution, and reproductive success of coastal plants (Cohen et al., 2012; Gabler et al., 2017; Liu et al., 2017; Osland et al., 2016).

Modern climate change studies observed in instrumental records provide evidence of climate variations during the Holocene (Novello et al., 2012; Scarelli et al., 2017; Vuille et al., 2012). For instance, significant changes in frequency and magnitude of the ENSO (El Niño-Southern Oscillation) event in the tropics occurred during the Holocene (Cobb et al., 2003). Within the last millennium, climatic events such as the 'Little Ice Age' (LIA), from 380 to 50 cal. yr BP (Dillenburg et al., 2017; Matthews and Briffa, 2005), and the Medieval Climate Anomaly (MCA), between 950 and 750 cal. yr BP, have been identified in paleoclimate records throughout both the hemispheres (Stine, 1994), further of the modern climate warmer period (CWP) since the past century (Vuille et al., 2012).

In addition, some studies have shown the impacts of the post-glacial sea-level rise at the Brazilian littoral (Angulo et al., 2006; Bezerra et al., 2003; Martin et al., 2003; Suguio et al., 1985), which inundated inland valleys (Scheel-Ybert, 2000), causing changes in coastal depositional systems and also in mangrove area (Cohen et al., 2012; França et al., 2013).

[1]Laboratório de Oceanografia e Estudos Paleoambientais, Instituto Federal de Educação, Ciência e Tecnologia do Pará, Brazil
[2]Centro de Energia Nuclear na Agricultura, Universidade de São Paulo, Brazil
[3]Laboratório de Dinâmica Costeira, Universidade Federal do Pará, Brazil
[4]Laboratório de Anatomia e Ecologia Vegetal, Departamento de Ciências Biológicas, Universidade da Região de Joinville, Brazil
[5]Departamento de Física, Universidade Federal Fluminense, Brazil

Corresponding author:
Marlon Carlos França, Laboratório de Oceanografia e Estudos Paleoambientais, Instituto Federal de Educação, Ciência e Tecnologia do Pará, Av. Almirante Barroso, 1155, Marco, CEP 66090-020, Belém, Pará, Brazil.
Email: marlon.franca@ifpa.edu.br

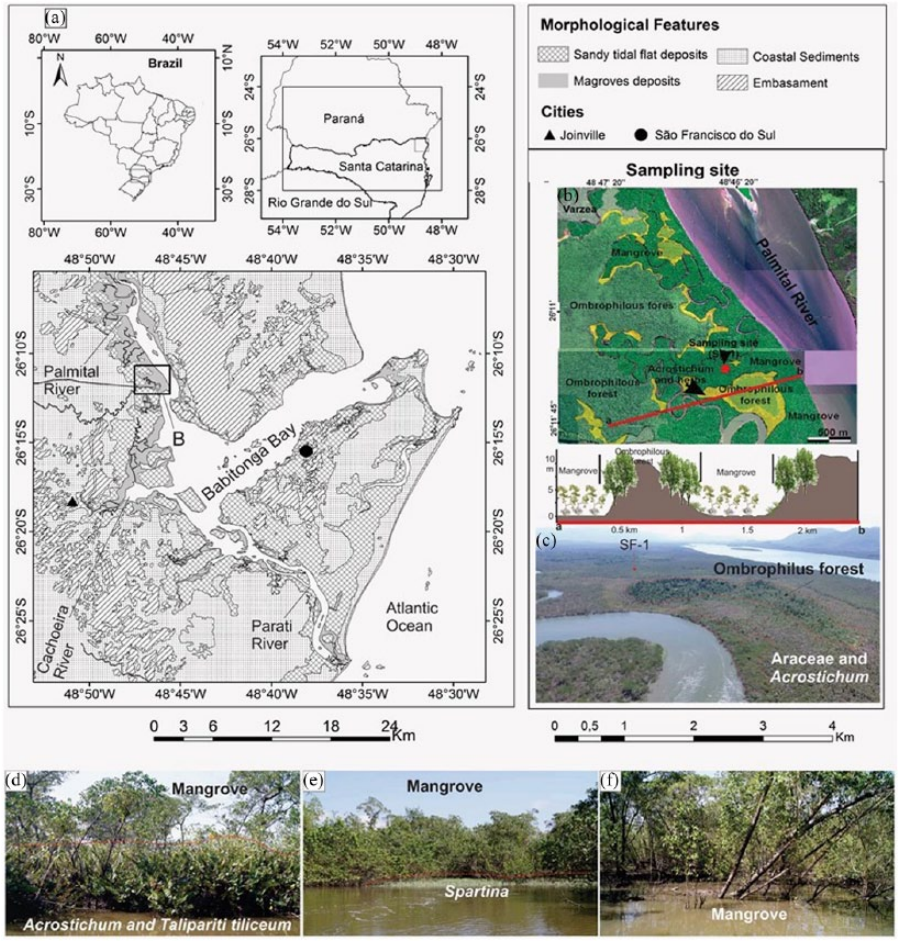

Figure 1. Location of the study area: (a) Brazil and State of Santa Catarina location (Instituto Brasileiro de Geografia e Estatística - IBGE, 2004; Mapa de Biomas e Vegetação do Brasil); (b) vegetation map, topographic profile and location of the sampling site; (c) sampling site highlighting the ombrophilous forest and *Araceae*/*Acrostichum* vegetation; (d) the contact between mangrove, *Acrostichum*, and *Taliparíti tiliaceum*; (e) mangrove and *Spartina* contact; and (f) the mangrove vegetation.

The expansion or contraction of mangrove areas depended on temperature, sediment type, salinity, inundation frequency, sediment accretion, and tidal and wave energy (Lugo and Snedaker, 1974). Specifically, the mangrove has special physiological and morphological adaptations that allow it to grow in intertidal environments (Alongi, 2008; Blasco et al., 1996). Thus, this ecosystem may be used as an indicator of environmental change (Blasco et al., 1996).

Recently, some studies have proposed that the global warming is affecting the latitudinal mangrove distribution (Coldren and Proffitt, 2017; Osland et al., 2016; Perry and Mendelssohn, 2009; Quisthoudt et al., 2012), since a rise in winter air temperature may be causing a mangrove expansion to the southern and northern latitudes of the American continent during the past decades (Cavanaugh et al., 2014; Giri and Long, 2014; Soares et al., 2012).

Along the Brazilian coast, mangroves are found from the extreme northern Brazilian coast in the Oiapoque River (04°20′N) to Laguna, State of Santa Catarina (28°30′S) in the southern coast (Schaeffer-Novelli et al., 2000). On the southern coast, mangroves are restricted to microtidal (tidal range below 2 m) bays, lagoons, or estuarine inlets, which are strongly controlled by climate and oceanographic characteristics (Soares et al., 2012).

Therefore, in order to determine the main forces driving the establishment and expansion of these subtropical mangroves on the Babitonga Bay, State of Santa Catarina, southern Brazil, this work studied a sediment core sampled from a mangrove area by sedimentary features, geochemistry analyses ($\delta^{13}C$, $\delta^{15}N$, TOC, TN, TS, C:N, and C:S ratio), pollen data, and radiocarbon dating.

Modern settings

Study area and geological setting

The study area is located on the mangrove tidal flat in the estuarine complex of Babitonga Bay (also named São Francisco do Sul Bay), State of Santa Catarina, southern Brazil (Figure 1), and presents a salt-wedge circulation system (Grace et al., 2008). The bay encompasses an area of approximately 167 km^2 with a coastline of 60 km between Barra do Sul and Itapoá (SC), including ~60 km^2 of well-preserved mangrove system (Instituto Brasileiro do Meio Ambiente e dos Recursos Naturais Renováveis (IBAMA), 1998). The Holocene history of this coastal system is strongly controlled by the relative sea level (RSL) changes and longshore transport (Angulo et al., 2009). In addition, this estuary is influenced by four hydrographic watersheds: Cachoeira River basin (85 km^2), Palmital River basin (358 km^2), Cubatão River basin (484 km^2), and Parati River basin (72 km^2) and it receives contributions from several minor streams (Barros et al., 2010).

The study area is characterized by Precambrian granites and a complex Paleozoic tectonic basement, volcanic associations, and Quaternary sedimentary deposits. The Precambrian substrate is composed of granitic-gneissic rocks of the Coastal Granitic Belt (Siga et al., 1993). These rocks reach the shore forming headlands and small islands. Low to high-grade metamorphic rocks are represented by schist, gneisses, and migmatite over the landward regions (Possamai et al., 2010). Crystalline massifs form the Serra do Mar coastal range and continental rift of southeastern Brazil (Riccomini, 1989), stretching from the State of Espírito Santo (~20°S) to the State of Santa Catarina (~28°S) (Dominguez,

2009). According to Giannini et al. (2009), uplifts occurred during the Cenozoic by a phase of gravitational collapse, creating several rifts parallel to the coast. The most prominent geomorphological characteristic is the scarped coastal range that, when intersecting the coastline, creates coastal embayments where strandplains and, less frequently, estuarine systems are found (Angulo et al., 2009), with evidence for the coastal depositional system formed during the Pleistocene and Holocene (Possamai et al., 2010). The Quaternary geology of the study area is characterized by Pleistocene and Holocene barriers, paleoestuarine plains, and tidal flats. The bay sector shows tidal flats with muddy sediments, beaches, succession of beach ridges, and parabolic dunes (Angulo et al., 2009).

Climatic and oceanographic setting

The region is characterized by a subtropical climate with wet summers and moderately dry winters (Cfa, according to Koppen's classification), mean annual precipitation and temperature from 1600 to 1900 mm and from 18 to 20°C, respectively (Alvares et al., 2014). It presents two differentiated seasons: summer (from November to April) and winter (from May to October). The interactions between tropical and extratropical atmospheric systems control the climate in southern Brazil (Nobre et al., 1986), with incursions of extratropical polar air masses related with cold fronts (Seluchi and Marengo, 2000). Cold fronts can bring wetter conditions to subtropical Brazil. In contrast, the warm-season precipitation (South Atlantic anticyclone), from late September to April, is associated with the activity of the South American Summer Monsoon (SASM; Cruz et al., 2006). An important feature of the SASM is the South American Convergence Zone (SACZ), a NW–SE elongated band of enhanced convective activity emanating from the Amazon River basin and extending into subtropical latitudes and over the South Atlantic Coast (Cruz et al., 2006).

The study area is characterized by microtidal, semidiurnal, ranging from 0.8 to 1.5 m (Fundação de Estudos do Mar (FEMAR), 2000). According to Cunha et al. (2005), water salinities are between 5.8 and 24. The coastal depositional system is wave-dominated with a tidal influence in the bay sector (Mazzer and Gonçalves, 2011). The shore may be classified as intermediate with an exposed beach (Klein and Menezes, 2001).

Vegetation

The region is composed mainly of tropical ombrophilous forest (Veloso et al., 1991), where the most representative plant families are Anacardiaceae (e.g. *Tapirira guianensis*), Arecaceae (e.g. *Euterpe edulis*), Asteraceae (e.g. *Vernonanthura montevidensis*), Bignoniaceae (e.g. *Jacaranda puberula*), Calophyllaceae (e.g. *Calophyllum brasiliense*), Chloranthaceae (e.g. *Hedyosmum brasiliense*), Euphorbiaceae (e.g. *Aparisthmium cordatum*), Fabaceae (e.g. *Schizolobium parahyba*), Lauraceae (e.g. *Ocotea pulchella*), Melastomataceae (e.g. *Tibouchina mutabilis*), Meliaceae (e.g. *Cabralea canjerana* and *Guarea macrophylla*), Myrtaceae (e.g. *Eugenia uniflora, Marlierea tomentosa, Myrcia splendens*, and *Psidium cattleianum*), Piperaceae (e.g. *Piper gaudichaudianum*), Rubiaceae (e.g. *Psychotria* spp.), and Urticaceae (e.g. *Cecropia catarinenses*). In the coastal plain, the vegetation is characterized by restinga where the most representative plant families are Asteraceae (e.g. *Baccharis singularis*), Bromeliaceae (e.g. *Aechmea gamosepala*), Dryopteridaceae (e.g. *Rumohra adiantiformis*) Fabaceae (e.g. *Dalbergia ecastaphyllum*), Mytaceae (e.g. *Marlierea tomentosa*), Rubiaceae (e.g. *Psychotria*) and Poaceae (e.g. *Lasiacis ligulata*). In addition, mangrove forests occur in the coastal plain, characterized by *Rhizophora mangle* (1.5–7 m height), *Laguncularia racemosa* (1–9 m height) and *Avicennia germinans* (3–4 m height), as well as Cyperaceae (e.g. *Schoenoplectus tabernaemontani*), Malvaceae (e.g. *Taliparitі tiliaceum*), Polypodiaceae (e.g. *Acrostichum aureum*), and Ruppiaceae (e.g. *Ruppia maritima*) (Cunha et al., 2005).

Materials and methods

Fieldwork and sampling processing

A LANDSAT 7 image (September 2002) was obtained from INPE (National Institute of Space Research, Brazil). A three-color band composition (RGB 543) image was created and processed using the SPRING 3.6.03 image processing system to discriminate geological features. Topographic data were derived from SRTM-90 data and downloaded from USGS Seamless Data Distribution System (https://dds.cr.usgs.gov/srtm/version2_1/SRTM3/). Image interpretation of elevation data was carried out using the software Global Mapper 12.

The fieldwork was carried out in September 2015. The sediment core SF-1 (3.00 m depth; S 26° 11' 20.90"/ W 48° 46' 29") was taken on fringe mangrove of the Palmital canal (Figure 1) using a Russian Peat Borer (USEPA, 1999). It is located approximately 20 km from the Atlantic Ocean on Babitonga Bay under fluvial, tide and wave influence (Mazzer and Gonçalves, 2011). The geographical position of this core was determined by GPS (Reference Datum: SAD69). High-definition images of the study area were obtained by a Drone Phantom 4 DJI with a 4 K/12MP camera. The drone survey was carried out by the DJI Ground Station Pro software. Eight predefined missions were implemented autonomously with a 90º camera angle, 90% frontal and lateral superimposition, and 100 m altitude.

Temperature and salinity

The temperature data were based on the Paranaguá Meteorological Station (25.53ºS and 48.51ºW; 4.50 m altitude), 70 km from the Babitonga Bay (SF-1 core), from 1961 to 2017. The data were downloaded from the National Institute of Meteorology (INMET/ http://www.inmet.gov.br). In order to obtain the general pattern of climate seasonality, temperature was calculated for the entire period considering a maximum, minimum temperature, and standard deviation. The SF-1 core was sampled during high tide (~1.6 m/ http://ondas.cptec.inpe.br). The salinity was 17‰ and the temperature of the water was 26°C.

Facies description

The core was X-rayed to identify sedimentary structures. Grain size was determined by laser diffraction using a Laser Particle Size SHIMADZU SALD 2101 in the Laboratory of Chemical Oceanography/UFPA. Prior to identifying the grain size, approximately 0.5 g of each sample was immersed in H_2O_2 to remove organic matter; and residual sediments were disaggregated by ultrasound. The sediment grain size distribution was determined following the methods of Wentworth (1922), with sand (2–0.0625 mm), silt (62.5–3.9 μm), and clay fraction (3.9–0.12 μm). The graphics were elaborated using the Sysgran Program (Camargo, 1999). Following the methods of Harper (1984) and Walker and James (1992), facies analysis included description of color (Munsell Color, 2009), lithology, texture, and structure. The sedimentary facies were codified following Miall (1978).

Palynological analysis

For pollen analysis 1.0 cm^3 samples were taken at 5-cm intervals downcore, for a total of 61 samples. All samples were prepared using standard pollen analytical techniques, including acetolysis (Faegri and Iversen, 1989). Sample residues were mounted on

Table 1. Sediment samples selected for radiocarbon dating and results with code site, laboratory number, depth (m), material, ages ^{14}C yr BP (1σ), calibrated ages (cal. yr BP, 2σ deviation), and median of calibrated ages (cal. yr BP).

Code site and laboratory number	Depth (m)	Material	Ages (^{14}C yr BP, 1σ)	Ages (cal. yr BP, 2σ deviation)	Median of age range (cal. yr BP)
UGAMS-28368	0.75–0.80	Bulk sed.	1070 ± 20	931–1005	968 ± 37
UGAMS-28372	1.10–1.15	Bulk sed.	950 ± 20	796–884	853 ± 44
UGAMS-28848	1.60–1.65	Bulk sed.	1570 ± 20	1402–1530	1469 ± 64
UGAMS-31233	2.30–2.35	Bulk sed.	1870 ± 30	1727–1875	1815 ± 74

slides in a glycerin gelatin medium. Pollen and spores were identified by comparison with reference collections of about 4000 Brazilian forest taxa and various pollen keys (Colinvaux et al., 1999; Markgraf and D'Antoni, 1978; Roubik and Moreno, 1991; Salgado-Labouriau, 1973) jointly with the reference collection of the Laboratory of Coastal Dynamics – Federal University of Pará and ^{14}C Laboratory of the Center for Nuclear Energy in Agriculture (CENA/USP) to identify pollen grains and spores. A minimum of 300 pollen grains were counted for each sample (except when pollen concentration was too low) to ensure the results are statistically significant. The total pollen sum excludes fern spores, algae, and foraminiferal tests. Pollen and spore data are presented in pollen diagrams as percentages of the total pollen sum. The *taxa* were grouped according to source: mangrove, herbs, trees and shrubs, and palms pollen, as well as of marine source (Foraminifera), ferns and fungi examples. The software TILIA and TILIAGRAF were used for calculation and to plot the pollen diagram (Grimm, 1990). CONISS was used for cluster analysis of pollen *taxa*, permitting the zonation of the pollen diagram (Grimm, 1987).

Isotopic and chemical analysis

A total of 132 samples (6–50 mg) were collected at 1–5 cm intervals from the sediment core. Sediments were treated with 5% HCl to eliminate carbonate, washed with distilled water until the pH reached 6, dried at 50ºC, and finally homogenized. These samples were analyzed for total organic carbon (TOC), total nitrogen (TN), stable isotopes of carbon and nitrogen, and total sulfur (TS) carried out at the 'Laboratório de Isótopos Estáveis' and 'Laboratório de Ciclagem de Nutrientes' of the Center for Nuclear Energy in Agriculture (CENA/USP), analyzed in an ANCA SL2020 mass spectrometer and Sulfur Analyzer SC 144DR-LECO, respectively. The standard for sulfur analysis was 0.031% (dry soil), from 0.028% to 0.034%. The results are expressed as a percentage of dry weight, with analytical precision of 0.09% (TOC), 0.07% (TN), and 0.02% (TS) respectively. The ^{13}C and ^{15}N results are expressed as δ^{13}C and δ^{15}N with respect to VPDB standard and atmospheric air, using the following notation:

$$\delta^{13}\mathrm{C}\ (‰) = \left[\left(R_{1\mathrm{sample}}/R_{2\mathrm{standard}}\right)\text{-}1\right] \times 1000$$

$$\delta^{15}\mathrm{N}\ (‰) = \left[\left(R_{3\mathrm{sample}}/R_{4\mathrm{standard}}\right)\text{-}1\right] \times 1000$$

where $R_{1\mathrm{sample}}$ and $R_{2\mathrm{standard}}$ are the ^{13}C/^{12}C ratio of the sample and standard, and $R_{3\mathrm{sample}}$ and $R_{4\mathrm{standard}}$ are the ^{15}N/^{14}N, respectively. Analytical precision is ±0.2‰ (Pessenda et al., 2004).

Surface sediment samples (1 cm) were collected to verify the isotopic composition of modern organic matter. Leaves of the most representative trees of the study area were also sampled for isotopic δ^{13}C determination to define photosynthetic characteristics of regional vegetation. The application of carbon isotopes is based on the ^{13}C composition of C_3 (trees) and C_4 (grasses) plants and its preservation in sedimentary organic matter (SOM).

Radiocarbon dating

Based on stratigraphic discontinuities that suggest changes in the tidal inundation regime, four bulk samples (10 g each) were selected for radiocarbon analysis. In order to avoid natural contamination by shells fragments, roots, seeds, etc., the sediment samples were checked and physically cleaned under the stereomicroscope. The organic matter was chemically treated to remove the presence of a younger organic fraction and to eliminate adsorbed carbonates by placing the samples in 2% HCl at 60°C for 4 h, followed by a rinse with distilled water to neutralize the pH. The samples were dried at 50ºC. A detailed description of the chemical treatment for sediment samples can be found in Pessenda et al. (2010, 2012). A chronologic framework for the sedimentary sequence was provided by conventional and accelerator mass spectrometer (AMS) radiocarbon dating. Samples were analyzed at the ^{14}C Laboratory of CENA/USP, LACUFF (Fluminense Federal University) and at UGAMS (University of Georgia – Center for Applied Isotope Studies). Radiocarbon ages were normalized to a δ^{13}C of −25‰ VPDB and reported as calibrated years (cal. yr BP; 2σ) using CALIB 7.1 (http://calib.org/calib/, accessed 3 November 2017; Reimer et al., 2013). The dates are reported in the text as the median of the range of calibrated ages (Table 1).

Results

Morphological and vegetation data

The study site presents 7 km^2 under influence of the Palmital river. The source of this river is in the Serra do Quirirí and it flows for 25 km until Babitonga Bay. The main tributaries are the Ounce, Sete Voltas, Bonito, Canela, Pirabeiraba, and Cubatão river. The drainage basin presents 358 km^2. The brackish water influence occurs along the studied stretch of the Palmital river that allow mangrove development (3 km^2) on tidal flats with porewater salinities between 7‰ and 20‰, characterized by *Rhizophora, Avicennia*, and *Laguncularia* trees. Upstream, muddy sediments are mainly dominated by 'várzea' vegetation (0.5 km^2; swampland seasonally inundated by freshwater) mainly represented by Arecaceae on flood plains with porewater salinities below 6‰. The limit between freshwater and mangrove vegetation is not always clearly fixed, because the transition between these vegetation units respond to a salinity gradient, where the vegetation, mainly characterized by Arecaceae (freshwater vegetation), is positioned upstream, while mangroves occupy zones under estuarine influence. The ombrophilous forest (2.5 km^2) occurs on elevated substrates without fluvial or tidal influence, while herbaceous vegetation, dominated by Poaceae, Cyperaceae, and Acrostichum, occurs on a topographic surface between mangrove and ombrophilous forest (Figure 1a), but some herbs also occupy low topographic levels, colonizing river banks.

Radiocarbon dates and sedimentation rates

The radiocarbon dates are shown in Table 1, with range since 1815 ± 74 cal. yr BP. The observed age inversions between 0.75–0.80 (968 ± 37 cal. yr BP) and 1.10–1.15 cm (853 ± 44 cal. yr BP) are probably related to high sedimentation rates and/or the root penetration and benthic organisms, resulting on input of younger organic matter from shallower depth into deeper layers. Radiocarbon dates obtained near the top of cores tend to present

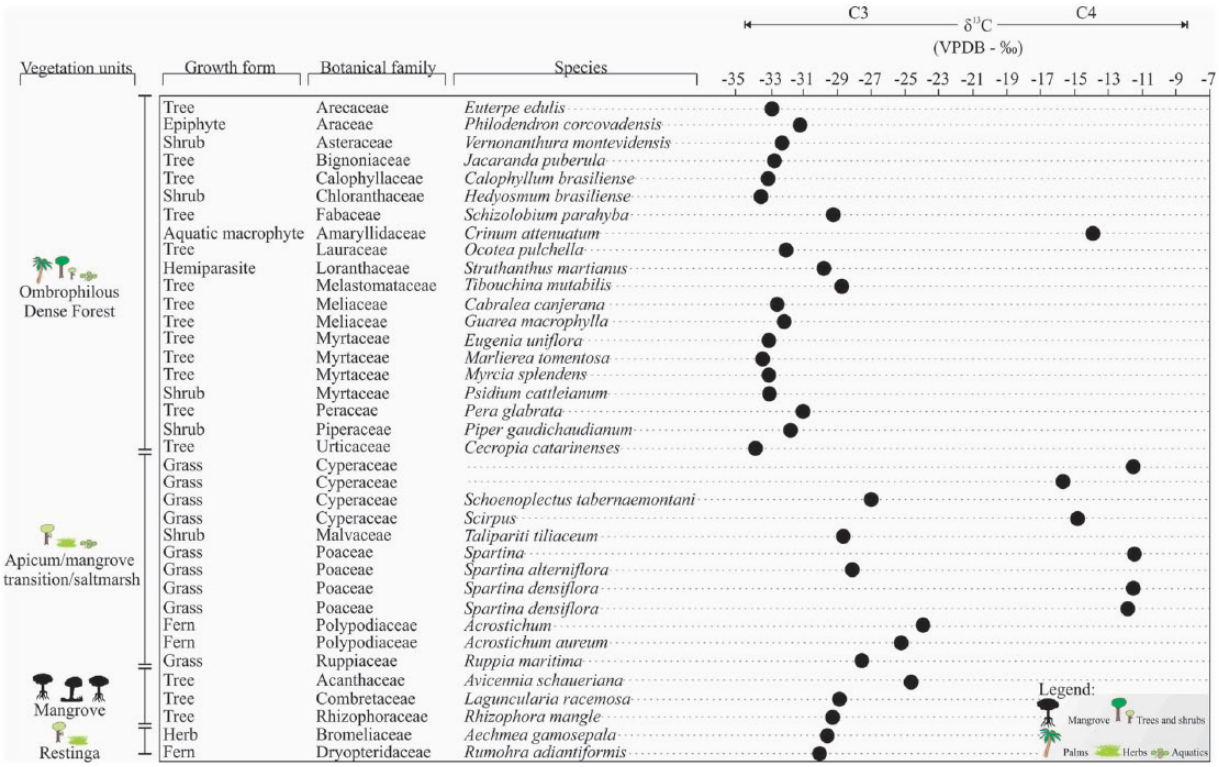

Figure 2. List of species and their $\delta^{13}C$ value sampled in the study site.

some imprecision usually caused by roots and bioturbation (ichnofossils), which can enhance the transport of allochthonous materials and contribute to date inversions (Cohen et al., 2014; Pessenda et al., 2012). Sedimentation rates have been obtained by Pb-210 and Cs-137 mainly in stagnant environments, such as lakes and water reservoirs (Baskaran et al., 2017). Sedimentation rates obtained by Pb-210 in tidal flats occupied by mangroves along Santa Catarina coast have shown conflicting results with sedimentation rates obtained by C-14, probably because of distinct sedimentary dynamics (Cohen, unpublished data). Based on radiocarbon dates, most of the cores with 3 m depth sampled from tidal flats occupied by mangroves reveal mean sedimentation rates of around 1 mm/year (Cohen et al., 2012), as evidenced along the studied core (Table 1). The estimated sedimentation rates were 2.0 mm/yr (2.35–2.30 to 1.65–1.60 m depth), 0.8 mm/yr (1.65–1.60 to 1.15–1.10 m depth) and 1.2 mm/yr (1.15–1.10 m depth up to the surface), with an extrapolated age of ~1630 yr BP at 1.95 m depth. Therefore, to analyze the events occurred during the last 50 cm, we have preferred to extrapolate the ages obtained by C-14 in the lower levels of the cores.

$\delta^{13}C$ values of modern vegetation

Thirty-seven species of the most representative vegetation were collected at the study site. The $\delta^{13}C$ values range between −33.84‰ and −11.5‰ and indicate a predominance of C_3 plants (Figure 2). The contribution of C_4 plants to the $\delta^{13}C$ signal in the sediment is restricted to the Amaryllidaceae (*Crinum attenuatum*), Cyperaceae (*Scirpus*), and Poaceae (*Spartina* and *Spartina densiflora*).

Facies, pollen description, and isotope values from sediment core

The sediments are composed mostly of olive gray and dusky yellow-green rippled sand. They present a fining upward into mixed deposits with sand (30%), silt (55%), and clay (15%) with low-angle planar laminations close to the top. The studied core shows leaf and root traces, and between 2.2 and 1 m depth shows shells trace. The sedimentary facies are characterized by massive sand (facies Sm), wavy heterolithic bedding (facies Hw), lenticular heterolithic bedding (facies Hl), and massive muddy deposits (facies Mm; Figure 3). The texture, grain size, sedimentary structures, and pollen contents, complemented with isotopic and geochemical data ($\delta^{13}C$, $\delta^{15}N$, TOC, TN, TS, C:N and C:S), define two facies associations representative of herbaceous tidal flat (A) and mangrove tidal flat (B).

Facies A (herbaceous tidal flat). Facies A occurs in the base of the sediment core since at least 1815 ± 74 cal. yr BP up to ~1630 yr BP (3.00–1.95 m depth, Figure 3). It consists mainly of massive sand (facies Sm) in the base grading upward into wavy heterolithic bedding (facies Hw) and lenticular heterolithic bedding (facies Hl). Some levels present rippled sand, cross-lamination (2.9 and 2.45 m depth), convolute-lamination (2.8 m depth), and low-angle planar lamination (2.3 m depth). Leaf and root fragments and shells are present.

The pollen and spore analysis revealed three ecological groups: herbs, trees and shrubs, and palms. In addition, foraminifera, ferns, and fungi were identified (Figure 4). The first pollen zone (SF1-A, Figure 4) is characterized mainly by herbaceous pollen (37–85%), represented by Cyperaceae (12–48%), Poaceae (10–40%), Amaranthaceae (2–12%), Asteraceae (2–11%) and Borreria (<5%). Trees and shrubs (12–47%) are represented by Anacardiaceae (1–17%), Euphorbiaceae (2–15%), and Fabaceae (~10%), further of Apocynaceae, Malpighiaceae, Malvaceae, Melastomataceae/Combretaceae, Myrtaceae, Rubiaceae, Sapindaceae with low percentages (<10%), followed by *Alchornea, Cecropia, Hedyosmum, Ilex*, and *Mimosa* also with low percentages (<8%). Palms are characterized by Arecaceae (2–18%). Mangrove pollen is not recorded along this facies association. Ferns and fungi are found, as well as marine markers.

The $\delta^{13}C$ and C/N values oscillated between −21 and −20‰ ($\bar{x}$ = −21.83‰), and 9.21 and 45.69 ($\bar{x}$ = 21.83) along the 300 and 240 cm interval, respectively. Between 240 and 195 cm, the $\delta^{13}C$ and C:N values stabilized about −27‰ and 20, respectively

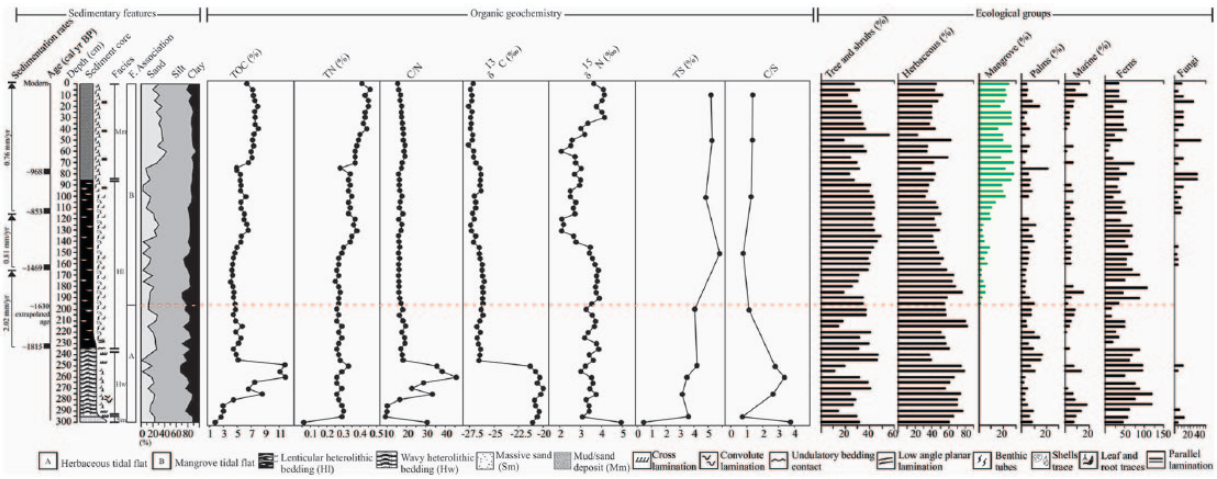

Figure 3. Summarized results for SF-1 core, with variation as a function of core depth showing chronological and lithological profiles with sedimentary facies, as well as ecological pollen groups and geochemical variables.

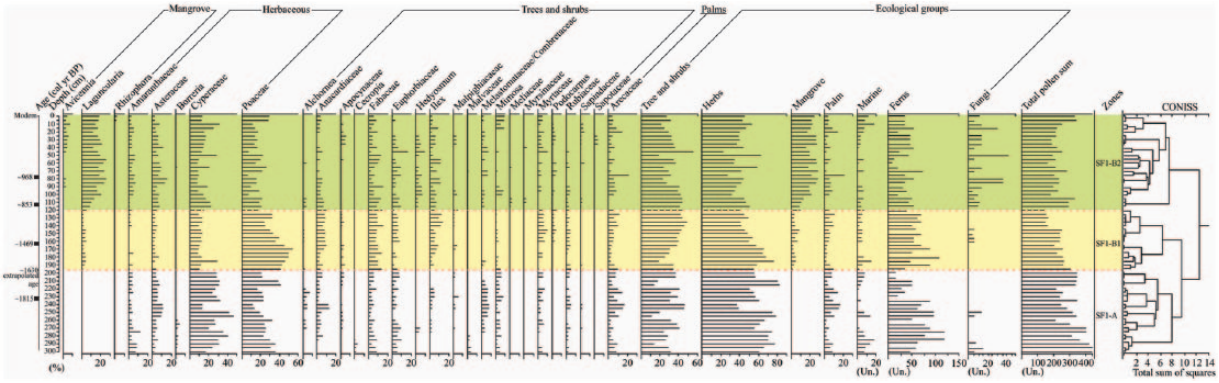

Figure 4. Pollen diagram record for SF-1 core, with percentages of the most frequent pollen taxa, samples age, zones, and cluster analysis.

(Figure 3). The $\delta^{15}N$ record shows values between 3.01‰ and 4.93‰ ($\bar{x}$ = 3.52‰) along the 300 and 195 cm interval, while the TOC and N results were between 1.8% and 11.9% ($\bar{x}$ = 5.7%) and 0.06–0.33% ($\bar{x}$ = 0.26%), respectively. The TS values were between 0.47% and 4.23% ($\bar{x}$ = 3.00%) and the C:S ratio results were between 0.47 and 4.23 ($\bar{x}$ = 2.44).

Facies association B (mangrove tidal flat). This facies association corresponds to the depth interval from 1.95 m (~1630 yr BP) up to the surface. These deposits consist of sandy-silt, silt, and clayey-silt sediments, revealing lenticular heterolithic bedding (facies Hl) and massive muddy deposits (facies Mm). Parallel laminations are observed toward the surface (Figure 3). Shells trace and dwelling structures produced by the benthic fauna are also visible, further of leaf and root traces.

The pollen assembly is characterized by four ecological groups, mainly defined by the establishment of mangrove (2–9%), between 1.95 and 1.20 m depth (SF1-B1, Figure 4), with an upward increased trend (10–28%; SF1-B2, Figure 4). The mangrove group is represented by *Laguncularia* (2–28%), *Avicennia* (2–8%), and *Rhizophora* (<5%), while herbaceous markers are characterized by Poaceae (8–55%), Cyperaceae (9–31%), Asteraceae (2–16%), Amaranthaceae (1–8%), and *Borreria* (~1%). Trees and shrubs are represented by Euphorbiaceae (2–18%), Fabaceae (2–16%), *Ilex* (2–12%), Anacardiaceae (2–10%), *Hedyosmum* (2–10%), *Mimosa* (2–10%), Myrtaceae (2–10%), Melastomataceae/Combretaceae (2–9%), Apocynaceae (2–6%), Sapindaceae (2–5%), Rubiaceae (1–5%), *Podocarpus* (2–6%), *Alchornea* (2–4%), Malpighiaceae (~4%), Sapotaceae (~3%), Meliaceae (1–2%), Myrsinaceae (~2%), and Malvaceae (<1%). The palms group, represented by Arecaceae, occurs between 2% and 21%. Ferns and fungi are found, further of marine markers (Foraminifera).

The $\delta^{13}C$ values exhibit a relatively stable result from −27.64‰ to −25.98‰ ($\bar{x}$ = –26.82‰) between 1.90 m and the surface. The $\delta^{15}N$ record shows an increased trend from 2.09‰ to 4.14‰ ($\bar{x}$ = 3.16‰), mainly between 130 and the surface. The TOC and TN results are between 4.05% and 8.02% ($\bar{x}$ = 6.00%) and 0.25–0.46% ($\bar{x}$ = 0.35%), respectively. The C:N values varied from 15.56 to 19.32 ($\bar{x}$ = 17.03). The TS and C:S data reveals values between 4.84% and 5.84% ($\bar{x}$ = 5.29%), and 0.8 and 1.4 ($\bar{x}$ = 1.21), respectively.

Interpretation and discussion

The pollen, sedimentary, and geochemical data suggest three phases of wetland development: (1) tidal flat colonized by herbs, palms, and trees and shrubs in the margin of the estuary (facies association A), where flow energy oscillated between medium and high flow regimes. In addition, the geochemical data showed organic matter was influenced by mixing C_3 and C_4 plants, macrophytes and marine particulate organic carbon (marine POC) between at least 1815 ± 74 cal. yr BP and ~1630 yr BP. The second phase (2) is characterized by the mangrove establishment represented by *Laguncularia* pollen between ~1630 yr BP and 853 ± 44 cal. yr BP, with an increased influence of C_3 plants and freshwater/estuarine dissolved organic matter (phytoplankton) (Figure 5). The third phase (3) is marked by mangrove expansion

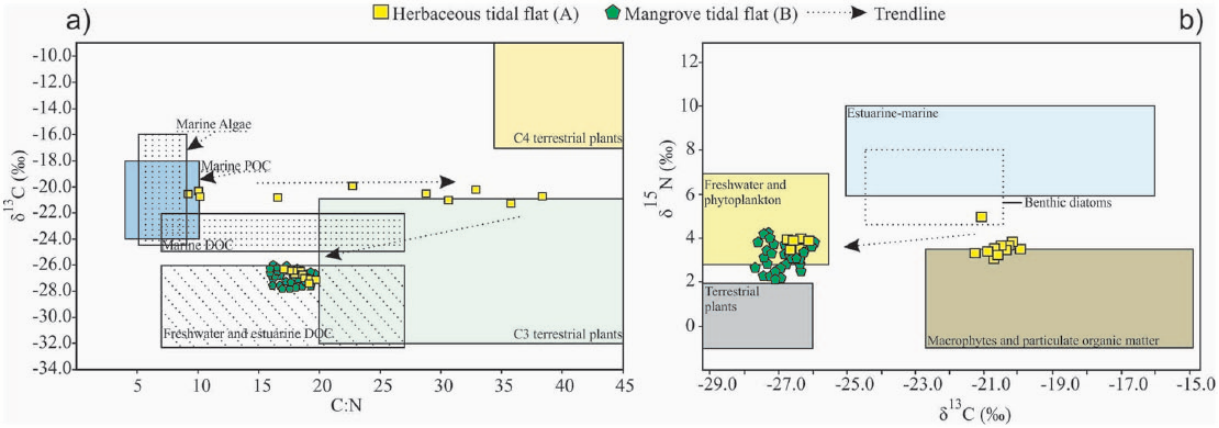

Figure 5. (a) Diagram illustrating the relationship between $\delta^{13}C$ versus C/N. (b) Diagram illustrating the relationship between $\delta^{15}N$ versus $\delta^{13}C$ for the different sedimentary facies (herbaceous tidal flat-A and mangrove tidal flat-B), with interpretation according to data presented by Meyers (2003) and Peterson and Howarth (1987) for the different organic matter source.

evidenced by the increase of *Laguncularia* trees, followed by *Avicennia* and *Rhizophora* trees, with influence of freshwater/estuarine dissolved organic matter and terrestrial plants (C_3 plants) during the last 853 ± 44 cal. yr BP (Figure 5).

First phase

This phase was initially marked by leaf and root traces in massive sand and wavy heterolithic bedding (Figure 3), which record high and medium flow energy with current action shaping the bedform characterized by oscillation ripples, cross lamination, and convolute lamination, produced by localized differential forces acting on a hydroplastic sediment layer, commonly found on mud flats (Collinson et al., 2006). Furthermore, this high flow energy induced the migration of small sand ripples (Reineck and Singh, 1980) and cross laminations close to 2.9 and 2.5–2.35 m depth. During this period, the margin of the estuary was occupied by herbs, palms, and trees and shrubs (Figure 4). Mangrove was not recorded during this period, despite the marine influence and appropriated muddy sediment accumulation (Pessenda et al., 2012). Also, during this period, the development of the herbaceous flat was largely represented by Cyperaceae (12–48%) and Poaceae (10–40%), which is associated with palms (until 18%), and trees and shrubs (10–45%). The enriched $\delta^{13}C$ values (−20‰) and the oscillation of C:N values (10–45), followed by upward decrease trends of $\delta^{13}C$ and C:N values from −19.98 to −26.73‰, and from 45 to 20, respectively, between 3.0 and 2 m depth, may be a result of C_4 herbaceous plants (between −17‰ and −9‰, Boutton and Yamasaki, 1996) associated with estuarine pulses during relative sea-level changes that contributed to the oscillations of aquatic organic matter influence in the base of the studied core. The mean value for C:S of 2.7 suggests a marine influence (Berner and Raiswell, 1984). Probably, the sedimentary organic matter of the studied core is responding to late-Holocene sea-level rise between 0.6 and 0.9 m above current sea level (Angulo et al., 2006; Milne et al., 2005). In addition, the binary diagrams between $\delta^{13}C \times$ C:N and $\delta^{15}N \times \delta^{13}C$ indicate a marine particulate organic carbon, mixture of C_3 and C_4 terrestrial plants, and macrophytes associated with estuarine/marine particulate organic matter, respectively (Figure 5). The mean value for $\delta^{15}N$ was 3.53‰, suggesting a mixture of terrestrial plants and aquatic organic matter (~5.0‰, Sukigara and Saino, 2005). Normally, the $\delta^{15}N$ of organic matter in the Brazilian forest areas near the ocean is around 3.13‰ (Martinelli et al., 2009). Variations in the nitrogen fixation rate from atmosphere, mineralization, nitrification, and denitrification determine the isotopic fractionation of nitrogen (Högberg, 1997).

Second phase

The sediment size and structures indicate a tidal flat marked by mid-energy flow. The relationship between $\delta^{13}C$ and C:N values (Figure 5) indicate a mixture of continental, dominantly composed of C_3 plants, and aquatic organic matter, composed of freshwater/estuarine dissolved organic carbon. The $\delta^{15}N$ values exhibit a mean value of around 3.23‰, suggesting an aquatic and terrestrial influence. However, close to the top of this phase, between 1.30 and 1.0 m depth, the mean value of $\delta^{15}N$ decreases to ~2.46‰ (2.09 to 2.77‰), which indicates an increase in terrestrial organic matter (~1‰, Peterson and Howarth, 1987). It may be related to the late-Holocene sea-level fall and stabilization registered around 1000 yr BP (Angulo et al., 2006) and/or a natural vertical accretion of sediments that contributes to the emergence of tidal flats and expansion of terrestrial vegetation. Normally, aquatic plants take up dissolved inorganic nitrogen, which is isotopically enriched in ^{15}N by 7‰ to 10‰ relative to atmospheric N (0‰), and thus terrestrial plants that use N_2 derived from the atmosphere have $\delta^{15}N$ values ranging from 0‰ to 2‰ (Meyers, 2003). The C:N ratio ($\bar{x}$ = 17.08) indicates an organic matter sourced mainly from vascular plants (>12 vascular plants, Meyers, 1994), probably because of herbs, and trees and shrubs occupation, as well as the *Laguncularia* trees establishment between ~1630 yr BP and 853 ± 44 cal. yr BP (Figure 4).

Third phase

The last phase is characterized by the expansion of *Laguncularia* trees on muddy tidal flats, followed by the *Avicennia* and *Rhizophora* trees establishment. The binary diagram of $\delta^{13}C$ versus C:N values (Figure 5) indicate C_3 plants and freshwater/estuarine organic matter influence. The mean value for C:S was 1.38 and indicates a marine influence (Berner and Raiswell, 1984), but the binary diagram $\delta^{13}C$ versus $\delta^{15}N$ (Figure 5) indicate a freshwater phytoplankton influence. Probably, mangroves were established under estuarine influence. It should be highlighted that $\delta^{13}C$ values of *Avicennia schaueriana, Laguncularia racemosa*, and *Rhizophora mangle* are about −27.79‰ (Figure 2). The TOC and N results show an increase from 4.91%to 8.02% and from 0.28%to 0.46%, respectively, probably because of mangrove expansion (Figure 4). The increase of $\delta^{15}N$ values from 2.08‰ to 4.14‰ ($\bar{x}$ = 3.21‰) suggest an increase in contribution of aquatic organic matter. The decrease trend of C:N values from 19.32 to 15.56 also indicate a similar influence.

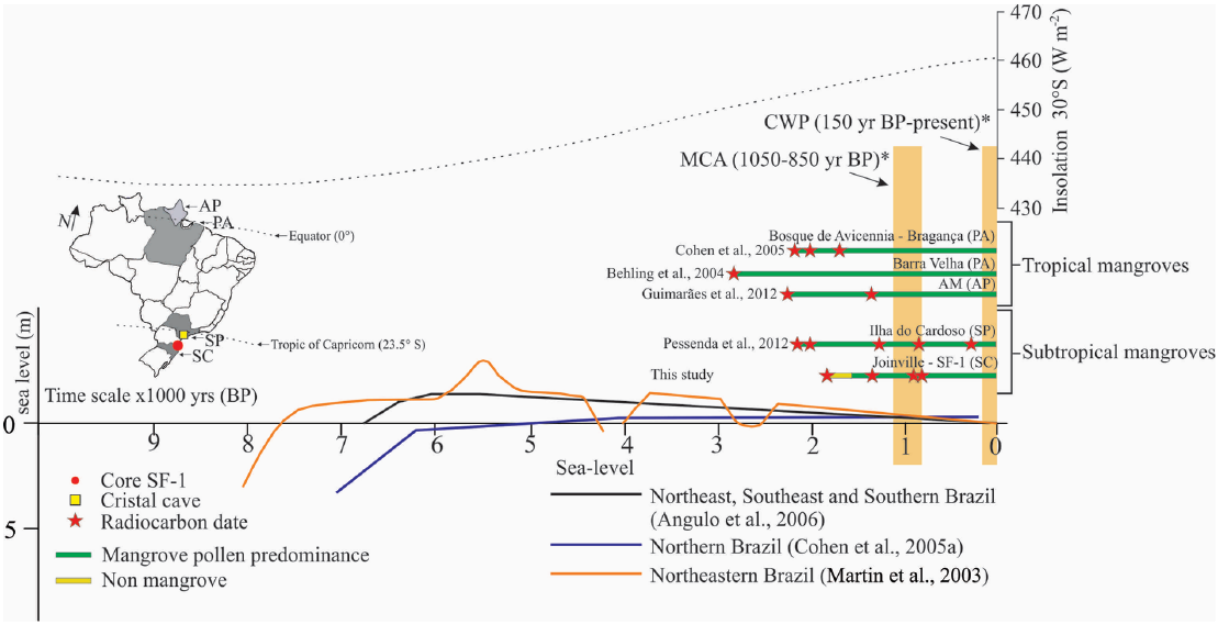

Figure 6. RSL curves of the eastern Brazilian coast during the Holocene with comparative pollen diagrams from Tropical and Subtropical mangroves, MCA (Medieval Climate Anomaly), CWP (Current Warm Period) and insolation 30°S (W.m^{-2}).

Latitudinal mangrove expansion during the late-Holocene

The studied pollen profile suggests that *Laguncularia* trees first appeared in a tidal flat during the second phase. It may indicate physical and chemical conditions suitable for mangrove establishment with marine influence as well as the salinity of 17‰ and the temperature of the water around 26°C measured in the study site. According to studied stratigraphic sequence, a tidal flat appropriate to mangrove development has been developed since at least 1815 ± 74 cal. yr BP, and only after 1630 yr BP, the pollen profile suggests a mangrove occupied only by *Laguncularia* trees up to 853 ± 44 cal. yr BP (Figure 4), followed by *Avicennia* and *Rhizophora* (Figure 4). Normally, in favorable climate conditions for the establishment of *Laguncularia, Avicennia*, and *Rhizophora* trees, a natural mangrove succession begins with herbaceous vegetation, such as *Spartina*, as a potential initial stabilizer, reducing erosion and to prepare a substrate favorable for the settlement of *Laguncularia*, creating the hydrodynamic conditions for mud accumulation and subsequent *Rhizophora* colonization, favoring the vertical accretion of sediments, and finally *Avicennia* trees occur when the sediments have already emerged enough to create conditions of low tidal flooding frequency and relatively high salinity (Tomlinson, 1986).

However, the studied pollen profile reveals initially the establishment of *Laguncularia*, later *Avicennia*, and finally, *Rhizophora* trees, which have different ranges of temperature and salinity tolerance (Quisthoudt et al., 2012). Therefore, we propose the establishment of *Laguncularia* during the second phase and its expansion, followed by establishment of *Avicennia* and *Rhizophora* trees during the third phase as a response to an increased trend of temperatures during the late-Holocene, driving the mangrove migration to southern latitudes along the Brazilian littoral (Figure 6). In this case, the recent expansion of *Rhizophora* trees in the study area originates from the northern coast (tropical zone), where the climatic conditions are more favorable for the red mangrove establishment. According to this hypothesis and considering the temperature gradients along the latitudes, the further north the Brazilian coast, the older was the mangrove establishment. A core sampled from São Paulo littoral (400 km north of the studied area and positioned in 25º S) recorded mangroves on tidal flats since at least ~2200 cal. yr BP (Pessenda et al., 2012), while mangroves between Linhares – Espírito Santo (1400 km north of the studied area) and Amapá, Northern Brazilian littoral were established at about 7000 cal. yr BP along a tropical zone with temperatures suitable for mangrove development during the Holocene (Cohen et al., 2012, 2014; França et al., 2013).

Regarding the temporal difference for the mangrove establishment at about 570 years between northern Santa Catarina and southern São Paulo littoral, a subtropical zone, it should be related to the gradual increase of temperature up to that littoral reaching the tolerance temperature range for the mangrove trees, where northern latitudes reach this range first. This late-Holocene warming may be associated with the Medieval Climate Anomaly (MCA, 1050–850 yr BP) and Current Warm Period (CWP, over the past ~100 yr), (Novello et al., 2012; Vuille et al., 2012). In addition, the South Atlantic shows a progressive increase in the sea surface temperature (SST) during the Holocene, with a prominent shift occurring during the mid- to late-Holocene that may be linked to changes in insolation distribution (Santos et al., 2013).

Avicennia is the most cold-tolerant genus worldwide (Stuart et al., 2007). *Avicennia germinans* has extended along the US Atlantic coast and expanded into salt marsh as a consequence of lower frost frequency and intensity in the southern US (Cavanaugh et al., 2014). Considering the coast of the Santa Catarina state, at Joinville (26º 12’ S) and near the study area (Figure 1), mangroves are represented by *Rhizophora, Avicennia*, and *Laguncularia* trees. The density of *Rhizophora* trees decrease toward the south until they are completely absent. The austral mangrove limit of the American continent occurs south of Santa Catarina (28º 30’ S) and is characterized mainly by *Laguncularia* trees with a few *Avicennia* shrubs. This distribution of mangrove genera along the Santa Catarina coast suggests a gradual tolerance to low temperatures of winter, where *Laguncularia* would be more tolerant and *Rhizophora* less adapted to low temperatures of winter. Then, the succession in establishment and expansion of mangrove types during the past 1000 years can have been caused by a linear increase in temperature during this time, where the temporal sequence in the establishment of this genus reflects the modern distribution of mangrove types along the coast of Santa Catarina. Alternatively, it should be noted that expansion of *Laguncularia* and establishment of *Avicennia*, followed by *Rhizophora* may

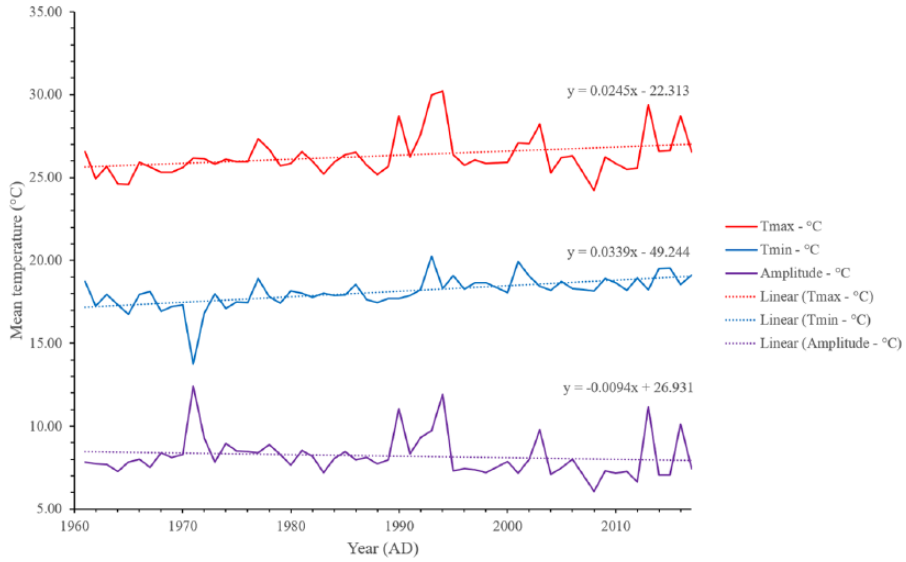

Figure 7. Maximum, minimum, and amplitude of the air temperature from 1961 to 2017 (Paranaguá Meteorological station − 25.53°S and 48.51°W; 4.50 m altitude).

have occurred during the MCA, LIA, and CWP, respectively. Considering that succession in the mangrove types is synchronized with these climatic events and *Avicennia* would be more tolerate to low temperatures than *Laguncularia*, the expansion of *Avicennia* trees during the LIA can have been caused by a decrease in the temperature. However, the LIA Brazilian record was associated with warm climatic inferences in the Southern region (Behling et al., 2004; Pessenda et al., 2010). In this case, the increased trend in temperature over the last 1000 years may not have been linear, and such succession in the mangrove types could have been controlled by oscillations in the temperature.

The variation of the SST was probably provoked by fluctuations of solar activity levels, which produced a cold period (Lean and Rind, 1999), like the LIA and warm period (CWP) during the late-Holocene (Novello et al., 2012). Climatic studies also revealed warming events since the last glacial maximum (LGM) period (Severinghaus and Brook, 1999) and wetter climate conditions during the last 2000 years (Sallun et al., 2012). The Holocene climate humidification would be related basically to attenuation of the contrast between the dry and humid seasons. A gradational increase in the mean temperatures would have been influenced by the minor frequency and intensity of the polar air masses (Wang et al., 2006). However, these events are regionally complex (Bradley et al., 2003; Jones and Mann, 2004) and their timing, magnitude, and natures have not been clearly delineated in South America (Moy et al., 2009).

The late-Holocene climate has been discussed for different paleoclimatic archives from the Southern Hemisphere, including Antarctic paleotemperature datasets (Blunier and Brook, 2001), diatom assemblages from South Atlantic marine sedimentary sequences (Smol and Stoermer, 2010), stalagmites data (Novello et al., 2016), the marine record from the tropical western Atlantic (Arz et al., 2001), and continental ice cores and lacustrine sequence datasets from South America (Lamy et al., 2001), with a millennial-scale warming trend on South America (Baker and Fritz, 2015).

The warming effects on mangrove distribution have been proposed (Coldren and Proffitt, 2017; Osland et al., 2016; Perry and Mendelssohn, 2009; Quisthoudt et al., 2012), and a mangrove expansion to southern latitudes of Brazil mainly during the past decades should be occurring because of decrease of frequency of low-temperature events (Soares et al., 2012). Paranaguá Meteorological Station (25.53ºS and 48.51ºW, 4.50 m altitude), 70 km from the Babitonga Bay (SF-1 core), from 1961 to 2017 has showed a mean maximum temperature of 26.09ºC ± 3.04 and the mean minimum of 18.06ºC ± 3.15, with a mean amplitude around 7.97ºC ± 1.92 during the past five decades, where a maximum and minimum temperature have increased, and the amplitude has decreased (Figure 7), favoring the mangrove, because that ecosystem has better development in regions with mean temperature above 20ºC and the annual thermal amplitude less than 5ºC (Chapman, 1975; Tomlinson, 1986).

Recently, a global prediction indicated a higher surface air temperature ranging from 1 to 3.7ºC (Collins et al., 2013). Global air temperature anomalies, based on instrumental records, compared with the average of a set of simulations show an increase in temperature (IPCC, 2001). Bernardino et al. (2015) showed data from Brazilian coastal regions with an increased frequency of positive temperature anomalies. Warmer years were more frequent and marked in the Brazilian coastal region, with yearly peaks of 1.5ºC above mean temperatures (Bernardino et al., 2015). Marengo (2006) estimated a mean temperature increase of 3 to 5°C in southern Brazil until AD 2080, probably in response to increasing concentrations of greenhouse gases. Therefore, following these climatic data and the pollen profile studied, we believe that mangroves may expand to more southern limits of the Brazilian coast, replacing herbaceous vegetation by mangroves on tidal flats and increasing the biodiversity with species of low climate tolerance such as *Rhizophora*.

Conclusion

Climatic changes caused by regional or global factors have significantly affected the mangrove forests during the late-Holocene. Probably, our data show the mangrove response to a Holocene air/water warming. During the first phase (since at least 1815 ± 74 until ~1630 yr BP) mangrove was not recorded in the study site, despite marine influence and appropriated muddy sediment accumulation during this period. The margin of the estuary was occupied by herbs, palms, and trees and shrubs. However, the subsequent phases, after ~1630 cal. yr BP, *Laguncularia* trees were established on tidal flats. At about 853 ± 44 cal. yr BP *Avicennia* expanded together with *Laguncularia* trees. Finally, during the past decades, *Rhizophora* trees also have occurred along the studied coast because of suitable climate conditions under a subtropical zone, caused by a continuous increase of temperature.

However, despite these results and considering the several forces that may influence mangrove dynamics, further detailed studies in other areas, consisting of the monitoring of mangrove forests, including fieldworks, are still needed in order to identify the influence of climate change on the distribution of mangroves along southern Brazil.

Acknowledgements

The authors would like to thank the members of the Laboratory of Costal Dynamic (LADIC-UFPA), Center for Nuclear Energy in Agriculture (CENA-USP), University of Joinville (UNIVILLE), the students from Laboratory of Chemical-Oceanography (UFPA), Laboratory of C-14 (CENA-USP), and Laboratory of Oceanography and Paleoenvironmental Studies (IFPA), for their support.

Funding

This study was financed by CNPq (445111/2014-3, 405060/2013-0) and FAPESP (2011/00995-7, 2017/03304-1). The first author would like to thank CNPq for research scholarship (Process 165911/2015-8 and 305074/2017-2).

ORCID iD


Marlon C França https://orcid.org/0000-0002-3784-7702

References

Alongi DM (2008) Mangrove forests: Resilience, protection from tsunamis, and responses to global climate change. *Estuarine, Coastal and Shelf Science* 76: 1–13.

Alvares CA, Stape JL, Sentelhas PC et al. (2014) Köppen's climate classification map for Brazil. *Meteorologische Zeitschrift* 22(6): 711–728.

Angulo RJ, Lessa GC and Souza MC (2006) A critical review of mid- to late-Holocene sea-level fluctuations on the eastern Brazilian coastline. *Quaternary Science Reviews* 25: 486–506.

Angulo RJ, Lessa GC and Souza MC (2009) The Holocene Barrier Systems of Paranaguá and Northern Santa Catarina Coasts, Southern Brazil. In: Dillenburg S and Hesp P (eds) *Geology and Geomorphology of Holocene Coastal Barriers of Brazil*. Berlin: Springer-Verlag, pp. 135–176.

Arz HW, Gerhardt S, Pätzold J et al. (2001) Stable oxygen isotope record and Calcium concentrations of sediment core GeoB3910–2. *PANGAEA*. Available at: https://doi.org/10.1594/PANGAEA.735159.

Baker PA and Fritz S (2015) Nature and causes of Quaternary climate variation of tropical South America. *Quaternary Science Reviews* 124: 31–47.

Barros GV, Martinelli LA, Novais TMO et al. (2010) Stable isotopes of bulk organic matter to trace carbon and nitrogen dynamics in an estuarine ecosystem in Babitonga Bay (Santa Catarina, Brazil). *Science of the Total Environment* 408(10): 2226–2232.

Baskaran M, Bianchi TS and Filley TR (2017) Inconsistencies between 14C and short-lived radionuclides-based sediment accumulation rates: Effects of long-term remineralization. *Journal of Environmental Radioactivity* 174: 10–16.

Behling H, Pillar VP, Orlóci L et al. (2004) Late Quaternary Araucaria forest, grassland (Campos), fire and climate dynamics, studied by high-resolution pollen, charcoal and multivariate analysis of the Cambará do Sul in Southern Brazil. *Palaeogeography, Palaeoclimatology, Palaeoecology* 203(3–4): 277–297.

Bernardino AF, Netto SA, Pagliosa PR et al. (2015) Predicting ecological changes on benthic estuarine assemblages through decadal climate trends along Brazilian Marine Ecoregions. *Estuarine, Coastal and Shelf Science* 166: 74–82.

Berner RA and Raiswell R (1984) C/S method for distinguishing freshwater from marine sedimentary rocks. *Geology* 12: 365–368.

Bezerra FHR, Barreto AMF and Suguio K (2003) Holocene sea-level history on the Rio Grande do Norte State coast, Brazil. *Marine Geology* 196: 73–89.

Blasco F, Saenger P and Janodet E (1996) Mangrove as indicators of coastal change. *Catena* 27: 167–178.

Blunier T and Brook EJ (2001) Timing of millennial-scale climate change in Antarctica and Greenland during the last glacial period. *Science* 291: 109–112.

Boutton TW and Yamasaki SI (1996) *Mass Spectrometry of Soils*. New York: Marcel Dekker.

Bradley RS, Vuille M, Hardy DR et al. (2003) Low latitude ice cores record Pacific sea surface temperatures. *Geophysical Research Letters* 30(4): 1174.

Camargo MG (1999) *Software para análise granulométrica SysGran, versão 3.0*. Curitiba: UFPR.

Cavanaugh KC, Kellner JR, Forde AJ et al. (2014) Poleward expansion of mangroves is a threshold response to decreased frequency of extreme cold events. *Proceedings of the National Academy of Sciences of the United States of America* 111(2): 723–727.

Chapman VJ (1975) Mangrove biogeography. *Proceedings of the Symposium on Biology and Management of Mangroves* 1: 3–22.

Cobb KM, Charles CD, Cheng H et al. (2003) El Niño/Southern Oscillation and tropical Pacific climate during the last millennium. *Nature* 424(17): 271–276.

Cohen MCL, França MC, Rossetti DF et al. (2014) Landscape evolution during the late Quaternary at the Doce River mouth, Espírito Santo State, Southeastern Brazil. *Palaeogeography, Palaeoclimatology, Palaeoecology* 415: 48–58.

Cohen MCL, Pessenda LCR, Behling H et al. (2012) Holocene palaeoenvironmental history of the Amazonian mangrove belt. *Quaternary Science Reviews* 55: 50–58.

Coldren GA and Proffitt CE (2017) Mangrove seedling freeze tolerance depends on salt marsh presence, species, salinity and age. *Hydrobiologia* 803(1): 159–171.

Colinvaux P, De Oliveira PE and Patiño JEM (1999) *Amazon Pollen Manual and Atlas*. Dordrecht: Harwood Academic Publishers.

Collins M, Knutti J, Arblaster JL et al. (2013) Long-term climate change: Projections, commitments and irreversibility. In: Stocker TF, Qin D, Plattner G-K et al. (eds) *Climate Change 2013: The Physical Science Basis. Contribution of Working Group I to the Fifth Assessment Report of the Intergovernmental Panel on Climate Change*. Cambridge and New York: Cambridge University Press, pp. 1029–1136.

Collinson J, Mountney N and Thompson D (2006) *Sedimentary Structures*. Edinburgh: Dunedin Academic Press.

Cruz FW, Burns SJ, Karmann I et al. (2006) Reconstruction of regional atmospheric circulation features during the late Pleistocene in subtropical Brazil from oxygen isotope composition of speleothems. *Earth and Planetary Science Letters* 248: 494–506.

Cunha SR, Tognella -de-Rosa MMP and Costa CSB (2005) Structure and litter production of mangrove forests under different tidal influences in Babitonga Bay, Santa Catarina, Southern Brazil. *Journal of Coastal Research* 39: 1169–1174.

Dillenburg S, Barboza EG, Rosa MLCC et al. (2017) The complex prograded Cassino barrier in southern Brazil: Geological and morphological evolution and records of climatic, oceanographic and sea-level changes in the last 7–6 ka. *Marine Geology* 390: 106–119.

Dominguez JML (2009) The coastal zone of Brazil. In: Dillemburg SR and Hesp PA (eds) *Geology and Geomorphology of Holocene Coastal Barriers of Brazil*. Berlin: Springer-Verlag, pp. 17–52.

Faegri K and Iversen J (1989) *Textbook of Pollen Analysis*. Chichester: Wiley.

Flantua SGA, Hooghiemstra H, Vuille M et al. (2016) Climate variability and human impact in South America during the last 2000 years: Synthesis and perspectives from pollen records. *Climate of the Past* 12: 483–523.

França MC, Cohen MCL, Pessenda LCR et al. (2013) Mangrove vegetation changes on Holocene terraces of the Doce River, Southeastern Brazil. *Catena* 110: 59–69.

Fundação de Estudos do Mar (FEMAR) (2000) *Catálogo de Estações Maregráficas Brasileiras*. Rio de Janeiro: FEMAR.

Giannini PCF, Guedes CCF, Nascimento DR Jr et al. (2009) Sedimentology and morphological evolution of the Ilha Comprida Barrier system, southern São Paulo coast. In: Dillemburg SR and Hesp PA (eds) *Geology and Geomorphology of Holocene Coastal Barriers of Brazil*. Berlin: Springer-Verlag, pp. 177–224.

Giri CP and Long J (2014) Mangrove reemergence in the northernmost range limit of eastern Florida. *Proceedings of the National Academy of Sciences of the United States of America* 111(15): E1447–E1448.

Glaber CA, Osland MJ, Grace CL et al. (2017) Macroclimatic change expected to transform coastal wetland ecosystems this century. *Nature Climate Change* 7: 142–147.

Grace VB, Mas-Pla J, Novais TO et al. (2008) Hydrological mixing and geochemical processes characterization in an estuarine/mangrove system using environmental tracers in Babitonga Bay (Santa Catarina, Brazil). *Continental Shelf Research* 28: 682–695.

Grimm EC (1987) CONISS: A FORTRAN 77 program for stratigraphically constrained cluster analysis by the method of the incremental sum of squares. *Computers & Geosciences* 13: 13–35.

Grimm EC (1990) TILIA and TILIAGRAPH: PC spreadsheet and graphic software for pollen data. *INQUA Sub-Commission on Data-Handling Methods Newsletter* 4: 5–7.

Hannah L and Bird A (2018) Climate change and biodiversity: Impacts. *Earth Systems and Environmental Sciences* 3: 249–258.

Harper CW (1984) Improved methods of facies sequence analysis. In: Walker RG and James NP (eds) *Facies Models – Response to Sea Level Change*. Ottawa: Geological Association of Canada, pp. 11–13.

Högberg P (1997) Tansley Review No. 95 15N natural abundance in soil-plant systems. *New Phytologist* 137: 179–203.

Instituto Brasileiro do Meio Ambiente e dos Recursos Naturais Renováveis (IBAMA) (1998) *Proteção e controle de ecossistemas costeiros: Manguezal da Baia de Babitonga* (Coleção meio ambiente. Série estudos – pesca). Brasilia: IBAMA.

Intergovernmental Panel on Climate Change (IPCC) (2001) *Climate Change: The Scientific Basis*. Cambridge: Cambridge University Press.

Jones PD and Mann ME (2004) Climate over past millennia. *Reviews of Geophysics* 42: RG2002.

Klein AHF and Menezes JT (2001) Beach morphodynamics and profile sequence for a Headland Bay Coast. *Journal of Coastal Research* 17(4): 812–835.

Lamy F, Hebbeln D, Röhl U et al. (2001) Holocene rainfall variability in southern Chile: A marine record of latitudinal shifts of the Southern Westerlies. *Earth and Planetary Science Letters* 185: 369–382.

Lean J and Rind D (1999) Evaluating Sun-climate relationships since the Little Ice Age. *Journal of Atmospheric and Solar-Terrestrial Physics* 61: 25–36.

Liu X, Conner WH, Song B et al. (2017) Forest composition and growth in a freshwater forested wetland community across a salinity gradient in South Carolina, USA. *Forest Ecology and Management* 389: 211–219.

Lugo AE and Snedaker SC (1974) The ecology of mangroves. *Annual Review of Ecology and Systematics* 5: 39–64.

Marengo JA (2006) *Mudanças climáticas globais e seus efeitos sobre a biodiversidade: caracterização do clima atual e definição das alterações climáticas para o território brasileiro ao longo do século XXI*. Brasilia: Ministério do Meio Ambiente.

Markgraf V and D'Antoni HL (1978) *Pollen Flora of Argentina*. Tucson, AZ: University of Arizona Press.

Martin L, Dominguez JML and Bittencourt ACSP (2003) Fluctuating Holocene sea levels is eastern and southeastern Brazil: Evidence from a multiple fossil and geometric indicators. *Journal of Coastal Research* 19: 101–124.

Martinelli LA, Ometto JPHB, Ferraz ES et al. (2009) *Desvendando Questões Ambientais com Isótopos Estáveis*. São Paulo: Oficina de Textos.

Matthews JA and Briffa KR (2005) The 'Little Ice Age': Re-evaluation of an evolving concept. *Geografiska Annaler, Series A: Physical Geography* 87A: 17–36.

Mayle FE, Burbridge R and Killeen T (2000) Millennial-scale dynamics of Southern Amazonian Rain Forests. *Science* 290: 2291–2294.

Mazzer AM and Gonçalves ML (2011) Aspectos geomorfológicos da baía de Babitonga, Santa Catarina, Brasil: Caracterização morfométrica. *Revista Brasileira de Geomorfologia* 12(3): 115–120.

Meyers PA (1994) Preservation of elemental and isotopic source identification of sedimentary organic matter. *Chemical Geology* 114: 289–302.

Meyers PA (2003) Applications of organic geochemistry to paleolimnological reconstructions: A summary of examples from the Laurentian Great Lakes. *Organic Geochemistry* 34: 261–289.

Miall AD (1978) Facies types and vertical profile models in braided river deposits: A summary. In: Miall AD (ed.) *Fluvial Sedimentology*. Calgary: Canadian Society of Petroleum Geologists, pp. 597–604.

Milne GA, Long AJ and Bassett E (2005) Modeling Holocene relative sea-level observations from the Caribbean and South America. *Quaternary Science Reviews* 24(10–11): 1183–1202.

Moy CM, Moreno PI, Dunbar RB et al. (2009) Climate change in southern South America during the last two millennia. In: Vimeux F, Sylvestre F and Khodri M (eds) *Past Climate Variability in South America and Surrounding Regions*. Dordrecht: Springer, pp. 353–393.

Munsell Color (2009) *Munsell Soil Color Charts*. New Revised Edition. New Windsor, NY: Macbeth Division of Kollmorgen Instruments.

Nobre CA, Cavalcanti IFA, Gan MA et al. (1986) Aspectos da climatologia dinâmica do Brasil. *Climanálise* Número especial, 124 pp.

Novello V, Cruz FW, Karmann I et al. (2012) Multidecadal climate variability in Brazil's Nordeste during the last 3000 years based on speleothem isotope records. *Geophysical Research Letters* 39: L23706.

Novello V, Vuille M, Cruz FW et al. (2016) Centennial-scale solar forcing of the South American Monsoon System recorded in stalagmites. *Nature Scientific Reports* 6: 24762.

Osland MJ, Enwright NM, Day RH et al. (2016) Beyond just sea-level rise: Considering macroclimatic drivers within coastal wetland vulnerability assessments to climate change. *Global Change Biology* 22(1): 1–11.

Perry CL and Mendelssohn IA (2009) Ecosystem effects of expanding populations of Avicennia germinans in a Louisiana Salt Marsh. *Wetlands* 29: 396–406.

Pessenda LCR, Gouveia SEM, Aravena R et al. (2004) Holocene fire and vegetation changes in Southeastern Brazil as deduced from fossil charcoal and soil carbon isotopes. *Quaternary International* 114: 35–43.

Pessenda LCR, Saia SEMG, Gouveia SEM et al. (2010) Last millennium environmental changes and climate inferences in the Southeastern Atlantic Forest, Brazil. *Anais da Academia Brasileira de Ciências* 82: 717–729.

Pessenda LCR, Vidotto E, De Oliveira PE et al. (2012) Late Quaternary vegetation and coastal environmental changes at Ilha do Cardoso mangrove record, Southeastern Brazil. *Palaeogeography, Palaeoclimatology, Palaeoecology* 363: 57–68.

Peterson BJ and Howarth RW (1987) Sulfur, carbon, and nitrogen isotopes used to trace organic matter flow in the salt-marsh estuary of Sapelo Island, Georgia. *Limnology and Oceanography* 32: 1195–1213.

Possamai T, Vieira CV, Oliveira FA et al. (2010) Geologia costeira da ilha de São Francisco do Sul, Santa Catarina. *Revista de Geologia* 2: 45–58.

Quisthoudt K, Schmitz N, Randin CF et al. (2012) Temperature variation among mangrove latitudinal range limits worldwide. *Trees: Structure and Function* 26: 1919–1931.

Reimer PJ, Bard E, Bayliss A et al. (2013) INTCAL13 and MARINE13 Radiocarbon age calibration curves, 0-50,000 years cal BP. *Radiocarbon* 55(4): 1869–1887.

Reineck HE and Singh IB (1980) *Depositional Sedimentary Environments with Reference to Terrigenous Clastics*. Berlin: Springer-Verlag.

Riccomini C (1989) *O Rift continental do sudeste do Brasil*. PhD Thesis, Universidade de São Paulo.

Roubik DW and Moreno JE (1991) *Pollen and Spores of Barro Colorado Island*. St. Louis, MO: Missouri Botanical Garden.

Salgado-Labouriau ML (1973) *Contribuição à palinologia dos cerrados*. Rio de Janeiro: Academia Brasileira de Ciências.

Sallun AEM, Filho WS, Suguio K et al. (2012) Geochemical evidence of the 8.2 ka event and other Holocene environmental changes recorded in paleolagoon sediments southeastern Brazil. *Quaternary Research* 77: 31–43.

Santos TP, Franco DR, Barbosa CF et al. (2013) Millennial-to centennial-scale changes in sea surface temperature in the tropical South Atlantic throughout the Holocene. *Palaeogeography, Palaeoclimatology, Palaeoecology* 392: 1–8.

Scarelli FM, Barboza EG, Cantelli L et al. (2017) Surface and subsurface data integration and geological modelling from the Little Ice Age to the present, in the Ravenna coastal plain, northwest Adriatic Sea (Emilia-Romagna, Italy). *Catena* 151: 1–15.

Schaeffer-Novelli Y, Cintrón G, Soares MLG et al. (2000) Brazilian mangroves. *Aquatic Ecosystem Health and Management* 3: 561–570.

Scheel-Ybert R (2000) Vegetation stability in the Southeastern Brazilian coastal area from 5500 to 1400 14C yr BP deduced from charcoal analysis. *Review of Paleobotany and Palynology* 110: 111–138.

Seluchi ME and Marengo JA (2000) Tropical-midlatitude exchange of air masses during summer and winter in South America: Climatic aspects and examples of intense events. *International Journal of Climatology* 20: 1167–1190.

Severinghaus JP and Brook EJ (1999) Abrupt climate change at the end of the last glacial period inferred from trapped air in polar ice. *Science* 286: 930–934.

Siga O, Basei MAS and Machiavelli A (1993) Evolução geotectônica da porção NE de Santa Catarina e SE do Paraná, com base em interpretações geocronológicas. *Revista Brasileira de Geociências* 23: 215–223.

Smol JP and Stoermer EF (2010) *The Diatoms: Applications for the Environmental and Earth Sciences*. Cambridge: Cambridge University Press.

Soares MLG, Estrada GCD, Fernandez V et al. (2012) Southern limit of the Western South Atlantic mangroves: Assessment of the potential effects of global warming from a biogeographical perspective. *Estuarine, Coastal and Shelf Science* 101: 44–53.

Stine S (1994) Extreme and persistent drought in California and Patagonia during Medieval time. *Nature* 369: 546–549.

Stuart SA, Choat B, Martin KC et al. (2007.) The role of freezing in setting the latitudinal limits of mangrove forests. *New Phytologist* 173: 576–583.

Suguio K, Martin L, Bittencourt ACSP et al. (1985) Flutuações do Nível do Mar durante o Quaternário Superior ao longo do Litoral Brasileiro e suas Implicações na Sedimentação Costeira. *Revista Brasileira de Geociências* 15: 273–286.

Sukigara C and Saino T (2005) Temporal variations of $\delta^{13}C$ and $\delta^{15}N$ in organic particles collected by a sediment trap at time-series station off the Tokyo Bay. *Continental Shelf Research* 25: 1749–1767.

Tomlinson PB (1986) *The Botany of Mangroves*. Cambridge: Cambridge University Press.

USEPA (1999) *Innovative Technology Verification Report: Sediment Sampling Technology, Aquatic Research Instruments Russian Peat Borer*. EPA/600/R-01/010. Washington, DC: Office of Research and Development.

Veloso HP, Rangel Filho ALR and Lima JCA (1991) *Classificação da Vegetação Brasileira, adaptada a um sistema universal*. Rio de Janeiro: IBGE.

Vuille MSJ, Burns BL, Taylor FW et al. (2012) A review of the South American Monsoon history as recorded in stable isotopic proxies over the past two millennia. *Climate of the Past* 8: 1309–1321.

Walker RG and James NP (1992) *Facies Models – Response to Sea Level Change*. Ottawa: Geological Association of Canada.

Wang X, Auler AS, Edwards RL et al. (2006) Interhemispheric anti-phasing of rainfall during the last glacial period. *Quaternary Science Reviews* 25: 3391–3403.

Wentworth CK (1922) A scale of grade and class terms for clastic sediments. *Journal of Geology* 30: 377–392.